The $(\alpha F^{357}C)_3(\beta R^{372}C)_3\gamma$ Subcomplex of the F_1-ATPase from the Thermophilic *Bacillus* PS3 Has Altered ATPase Activity after Cross-Linking α and β Subunits at Noncatalytic Site Interfaces†

Sanjay Bandyopadhyay, Huimiao Ren, Ching S. Wang, and William S. Allison*

Department of Chemistry and Biochemistry, University of California at San Diego, La Jolla, California 92093-0601

Received November 6, 2001; Revised Manuscript Received December 14, 2001

ABSTRACT: In crystal structures of bovine MF_1, the side chains of αF^{357} and βR^{372} are near the adenines of nucleotides bound to noncatalytic sites. To determine if during catalysis these side chains must pass through the different arrangements in which they are present in crystal structures, the catalytic properties of the $(\alpha F^{357}C)_3(\beta R^{372}C)_3\gamma$ subcomplex of the TF_1-ATPase were characterized before and after cross-linking the introduced cysteines with $CuCl_2$. The unmodified mutant enzyme hydrolyzes MgATP at 50% the rate exhibited by wild type. Detailed comparison of the catalytic properties of the double mutant enzyme before and after cross-linking with those of the wild-type subcomplex revealed the following. Before cross-linking, the $(\alpha F^{357}C)_3(\beta R^{372}C)_3\gamma$ subcomplex has less tendency than wild type to release inhibitory MgADP entrapped in a catalytic site during turnover when MgATP binds to noncatalytic sites. Following cross-linking, ATPase activity is reduced 5-fold, and inhibitory MgADP entrapped in a catalytic site during turnover does not release under conditions wherein binding of ATP to noncatalytic sites of the wild-type enzyme promotes release of MgADP from the affected catalytic site. When assayed in the presence of lauryldimethylamine oxide, which prevents turnover-dependent entrapment of inhibitory MgADP in a catalytic site, ATPase activity of the cross-linked form is 47% that of the unmodified mutant enzyme. These results suggest that, during catalysis, the side chains of αF^{357} and βR^{372} do not pass through the extremely different relative positions in which they exist at the three noncatalytic site interfaces in crystal structures.

The F_oF_1-ATP synthases couple proton translocation to the condensation of ADP with P_i in energy transducing membranes. The F_o sector is an integral membrane protein complex that mediates proton translocation. The catalytic sites for the condensation reside on the F_1 sector, a peripheral membrane protein complex comprised of five different polypeptides in $\alpha_3\beta_3\gamma\delta\epsilon$ stoichiometry. When removed from the membrane as a soluble complex, F_1 is an ATPase that contains six nucleotide binding sites. Three of these are catalytic sites, whereas the other three are called noncatalytic sites (*1*, *2*).

In the crystal structure of MF_1[1] deduced by Abrahams et al. (*3*), the α and β subunits are arranged alternately in a hexameric configuration, the central cavity of which is occupied with a coiled coil assembled from the amino and carboxyl termini of the γ subunit. The three noncatalytic sites in the crystal structure are located at α/β interfaces where MgAMP-PNP is bound mostly to α subunits that are folded in identical closed conformations. In contrast, catalytic sites, which are located at different α/β interfaces, are heterogeneously liganded. One, designated α_T/β_T, contains MgAMP-PNP bound mostly to β_T. MgADP is bound in a manner similar to that of another catalytic site, designated α_D/β_D. The third catalytic site is empty and is designated α_E/β_E. Whereas β_T and β_D have nearly identical closed conformations resembling those of α subunits, β_E has a very different open conformation. The amino acid side chains that interact with bound nucleotides or Mg^{2+} in the closed catalytic sites at the α_T/β_T and α_D/β_D interfaces are arranged very differently in the open catalytic site at the α_E/β_E interface.

Although it has been shown that modification of noncatalytic sites with the nucleoside analogue 5′-*p*-(fluorosulfonyl)-benzoyladenosine inactivates ATP hydrolysis catalyzed by isolated F_1-ATPases (*4*, *5*) and ATP synthesis catalyzed by submitochondrial particles (*6*), a precise functional role of these sites has not been elucidated. Studies with the isolated MF_1- and TF_1-ATPases have shown that occupancy of noncatalytic sites with ATP decreases propensity of the enzymes to entrap inhibitory MgADP in a catalytic site during turnover (*7*−*9*). The $(\alpha D^{269}N)_3\beta_3\gamma$ subcomplex[2] of TF_1, in which an aspartate that interacts with the Mg^{2+} component of MgAMP-PNP bound to noncatalytic sites is

† This study was supported by Grant GM-16974 from the U.S. Public Health Service to W.S.A.

* Corresponding author. Phone: 858-534-3057. Fax: 858-822-0079. E-mail: wsa@checfs2.ucsd.edu.

[1] Abbreviations: MF_1, TF_1, and EF_1, F_1-ATPases from bovine heart mitochondria, the thermophilic *Bacillus* PS3, ΔNC, the $(\alpha K^{175}A/T^{176}A/D^{269}A/D^{170}A)_3\beta_3\gamma$ subcomplex, and *E. coli* EF_oF_1, *Escherichia coli* ATP synthase; AMP-PNP, adenyl-5′-yl-(β,γ-imidophosphate); CDTA, *trans*-1,2-diaminocyclohexane-*N*,*N*,*N*′,*N*′-tetraacetic acid; DCCD, dicyclohexylcarbodiimide; DTT, dithiothreitol; DTNB, 5,5′-dithiobis(2-nitrobenzoic acid); TDAB, tetradecyltrimethylammonium bromide; LDAO, lauryldimethylamine oxide.

[2] Unless stated otherwise, residue numbers are those of bovine heart MF_1.

10.1021/bi0120291 CCC: $22.00
Published on Web 02/06/2002

substituted, fails to dissociate inhibitory MgADP from the affected catalytic site when MgATP binds to noncatalytic sites. This suggests that noncatalytic nucleotide binding sites in the wild-type enzyme are in conformational equilibrium with catalytic sites (*10*). The unusual catalytic properties of the ΔNC mutant $\alpha_3\beta_3\gamma$ subcomplex of TF_1, which does not bind nucleotides to noncatalytic sites, described by Matsui et al. (*11*) provided additional evidence that noncatalytic sites are involved in release of inhibitory MgADP entrapped in a catalytic site. This quadruple mutant, which contains four substitutions of amino acid in α subunits that interact with AMP-PNP bound to noncatalytic sites in the crystal structure of MF_1 (*3*), retains inhibitory MgADP in a catalytic site under conditions wherein binding of ATP to noncatalytic sites of the wild-type enzyme promotes release of inhibitory MgADP from the affected catalytic site.

Amino acid side chains that interact with the adenine of AMP-PNP bound to noncatalytic sites are arranged differently at the $\alpha_E\beta_D$, $\alpha_D\beta_T$, and $\alpha_T\beta_E$ noncatalytic site interfaces in crystal structures of MF_1 from bovine heart mitochondria. The nearest distances between C_ζ of αF^{357} and the guanidinium N_ζ of βR^{372} at the α_E/β_D, α_D/β_T, and α_T/β_E interfaces are 4.1, 4.6, and 8.6 Å, respectively, in the original crystal structure (*3*); 11.7, 4.5, and 6.8 Å, respectively, in the crystal structure in which Glu^{199} in β_D is derivatized with DCCD (*12*); and 4.1, 7.5, and 11.7 Å, respectively, in the most recent crystal structure in which MgADP−fluoroaluminate complexes are bound to catalytic sites at the α_T/β_T and α_D/β_D interfaces and MgADP is bound to the half-closed catalytic site at the α_E/β_E interface (*13*).

It has been established that, during ATP hydrolysis, the three catalytic sites of F_1-ATPases work in sequence driving counterclockwise rotation of the γ subunit in 120° increments as catalysis occurs at the individual sites (*14*, *15*). Substantial evidence suggests that each catalytic site and the β subunit in which it resides must cycle through completely open and completely closed conformations during catalysis (*13*, *16*). Therefore, it was of interest to find out if introduction of cross-links between α and β subunits at noncatalytic site interfaces might abolish ATP hydrolysis. To accomplish this, the catalytic properties of the $(\alpha F^{357}C)_3(\beta R^{372}C)_3\gamma$ double mutant subcomplex of TF_1 were examined in detail before and after forming disulfide bonds between introduced cysteines on one hand and carboxymethylation of the introduced cysteines on the other. The results and mechanistic implications of this study are reported here.

EXPERIMENTAL PROCEDURES

Generation and Expression of the Plasmid Encoding the $(\alpha F^{357}C)_3(\beta R^{372}C)_3\gamma$ Double Mutant Subcomplex. Plasmid pKK, which carries the genes encoding the α, β, and γ subunits of TF_1, was used for both site-directed mutagenesis and gene expression (*17*). Expression plasmids were constructed using the polymerase chain reaction and the QuickChange site-directed mutagenesis kit obtained from Stratagene. The plasmids were purified using the Wizard Plus miniprep kit from Promega. The primers along with their corresponding complements (not shown) that were used to incorporate the base changes were 5′-GCAATCGGACTTGTGCTTCTCCGGCGTC-3′ for the $\alpha F^{357}C$ substitution and 5′-CATTATCAAGTCGCCTGCAAAGTGCAGCAAACG-3′ for the $\beta R^{372}C$ substitution. The bases changed are underlined. The double mutant pKK plasmid was expressed in *Escherichia coli* strain JM103 (*unc*$^-$). Purification of the wild-type $\alpha_3\beta_3\gamma$ and $(\alpha F^{357}C)_3(\beta R^{372}C)_3\gamma$ double mutant subcomplexes was performed as described by Matsui and Yoshida (*17*). Purified enzymes were stored as suspensions in 75% saturated ammonium sulfate at 4 °C.

Removal of Endogenous Nucleotides from the Isolated Subcomplexes. Unless stated otherwise, solutions of the enzyme were prepared by dissolving pelleted ammonium sulfate precipitates obtained by centrifugation in 50 mM Tris-HCl, pH 8.0, containing 10 mM CDTA. After 30 min at 23 °C, 100 μL aliquots were passed through 1 mL centrifuge columns of Sephadex G-50 (*18*) equilibrated with 50 mM Tris-HCl, pH 8.0, containing 0.1 mM EDTA. In the case of the $(\alpha F^{357}C)_3(\beta R^{372}C)_3\gamma$ mutant destined for oxidation with $CuCl_2$, the column effluents were passed through a second 1 mL centrifuge column equilibrated with the same buffer in the absence of EDTA.

Analytical Methods. Endogenous nucleotides bound to the enzyme subcomplexes were determined by HPLC on a TSK-DEAE-5PW Sepharogel column equilibrated and eluted with 50 mM KH_2PO_4, pH 4.3, containing 120 mM NaCl (*19*). The CDTA-treated wild-type and mutant subcomplexes were essentially free of endogenous nucleotide. Protein concentrations were determined by the method of Bradford using Coomassie Blue from Pierce (*20*).

ATPase activity was determined spectrophotometrically in the presence of 2 mM ATP and 3 mM $MgCl_2$ using an ATP regeneration system with phosphoenolpyruvate and pyruvate kinase coupled to NADH oxidation by lactate dehydrogenase at 30 °C and pH 8.0. Unless stated otherwise, ATPase assays of the unmodified $(\alpha F^{357}C)_3(\beta R^{372}C)_3\gamma$ subcomplex were performed in the presence of 1 mM DTT in the assay medium. Radioactivity was determined by liquid scintillation counting in Ecoscint obtained from National Diagnostics.

Preparation of the Fully Reduced and Completely Oxidized $(\alpha F^{357}C)_3(\beta R^{372}C)_3\gamma$ Subcomplex. The fully reduced double mutant was prepared by treating the isolated subcomplex free of endogenous nucleotides at 1 mg/mL in 50 mM Tris-HCl, pH 8.0, with 10 mM DTT for 30 min at 23 °C, at which time DTT was removed by passing the reaction mixture through a Sephadex G-50 centrifuge column equilibrated with the same buffer. The fully oxidized enzyme was prepared by treating the double mutant free of endogenous nucleotides at 1 mg/mL in 50 mM Tris-HCl, pH 8.0, with 100 μM $CuCl_2$ at 23 °C for 30 min. The reaction mixture was then passed through a Sephadex G-50 centrifuge column equilibrated with the same buffer to remove excess Cu^{2+}.

Carboxymethylation of the Reduced $(\alpha F^{357}C)_3(\beta R^{372}C)_3\gamma$ Mutant Subcomplex. To a 1 mg/mL solution of the fully reduced form of the $(\alpha F^{357}C)_3(\beta R^{372}C)_3\gamma$ double mutant in 50 mM Tris-HCl, pH 8.0, was added iodo[^{3}H]acetate (American Radiolabeled Chemicals) adjusted to pH 7.0 with NaOH to a final concentration of 4 mM. The reaction mixture was incubated for 20 h at 23 °C, at which time excess iodo-[^{3}H]acetate was removed by passing it through a Sephadex G-50 centrifuge column equilibrated with 50 mM Tris-HCl, pH 8.0. Titration of the residual cysteine with DTNB after treating the reduced enzyme with iodo[^{3}H]acetate revealed

that only three of the introduced cysteines were derivatized (*21*).

Preparation of Tryptic Digests of the Reduced, Carboxymethylated, and Cross-Linked ($\alpha F^{357}C)_3(\beta R^{372}C)_3\gamma$ Subcomplex after Photolabeling with 2-N_3-[^{3}H]ADP. The three forms of the mutant complex were photoinactivated at 1 mg/mL with 150 μM 2-N_3-[^{3}H]ADP in the presence of 1 mM $MgCl_2$ as described by Jault et al. (*10*) until less than 15% activity remained. The photoinactivated enzymes were precipitated by addition of solid ammonium sulfate to a final concentration of 55% saturation. After centrifugation, the protein precipitates were dissolved in 6 M guanidine hydrochloride and treated with 10 mM DTT at 23 °C for 1.5 h, at which time iodoacetate was added to a final concentration of 20 mM. The reaction mixtures were incubated for 1 h at 23 °C, at which time they were submitted to dialysis against 2 L of deionized water with one change for 16 h at 23 °C. The carboxymethylated, photolabeled proteins precipitated during dialysis. However, the precipitates dissolved when they were subsequently collected by centrifugation and suspended in 1 mL of 50 mM Tris-HCl, pH 8.0, containing TPCK-trypsin (1/50 w/w) for 16 h at 23 °C.

Polyacrylamide Gel Electrophoresis. SDS−PAGE was performed on 12% gels. TDAB−PAGE was carried out essentially as described in Penin et al. (*22*) except that electrophoresis was performed on 12.5% gels equilibrated with 0.2 M NaH_2PO_4 at pH 4.0.

RESULTS

The ATPase Activity of the Reduced ($\alpha F^{357}C)_3(\beta R^{372}C)_3\gamma$ Double Mutant Is 50% That of Wild Type and Is Slightly More Sensitive to Turnover-Dependent Entrapment of Inhibitory MgADP. The $(\alpha F^{357}C)_3(\beta R^{372}C)_3\gamma$ subcomplex was isolated in partially cross-linked form as assessed by SDS−PAGE with a specific activity of 7 μmol of ATP hydrolyzed mg^{-1} min^{-1}. Treatment of the isolated enzyme with 10 mM DTT for 30 min at 23 °C prior to assay increased the specific activity to 10 μmol of ATP hydrolyzed mg^{-1} min^{-1} and eliminated cross-linking (see lane 1 of Figure 3).

Previous studies have shown that MF_1, TF_1, and the wild-type $\alpha_3\beta_3\gamma$ subcomplex of TF_1 hydrolyze 50 μM ATP in three kinetic phases (*8*−*10*) when assayed in the presence of an ATP regenerating system. Figure 1A illustrates that the wild-type and fully reduced double mutant subcomplexes hydrolyze 50 μM ATP with an initial burst that decelerates to an intermediate rate, which, in turn, slowly accelerates to a final rate that approaches the initial rate. Acceleration from the intermediate rate is less pronounced in the trace recorded for the fully reduced double mutant. The numbers at the end of the traces indicate the specific activities of the enzyme subcomplexes (μmol of ATP hydrolyzed mg^{-1} min^{-1}) determined from the rates recorded over the last 1 min.

In experiments not illustrated, after a single catalytic site of each enzyme was loaded with MgADP, 50 μM ATP was hydrolyzed with a lag that accelerated to the same final rate exhibited in Figure 1A for the traces obtained in the absence of additions. These and other observations described in detail previously suggest that deceleration from the initial rate is caused by turnover-dependent entrapment of inhibitory MgADP in a catalytic site and acceleration from the intermediate phase is caused by slow binding of ATP to noncatalytic sites that promotes dissociation of inhibitory MgADP from the affected catalytic site (*8*−*11*).

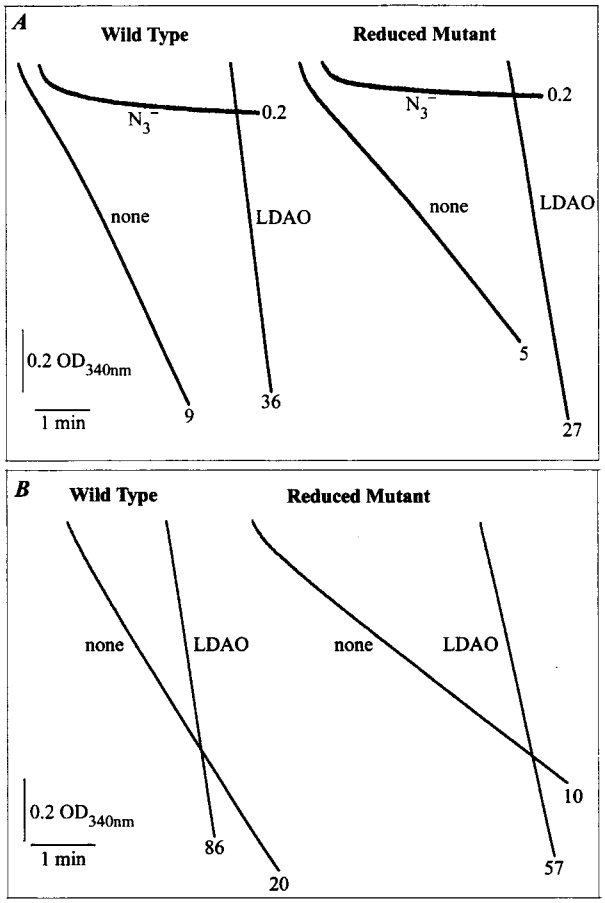

FIGURE 1: Comparison of the effects of azide and LDAO on hydrolysis of ATP by the wild-type and reduced $(\alpha F^{357}C)_3(\beta R^{372}C)_3\gamma$ enzymes. (A) Assays were conducted at 30 °C and were initiated by injecting 5 μg of the wild-type enzyme or reduced mutant enzyme into 1 mL of assay medium containing 50 μM ATP, 1.05 mM $MgCl_2$, 0.25 mM NADH, 20 units of pyruvate kinase, and 10 units of lactate dehydrogenase in 50 mM Hepes−KOH, pH 8.0, with and without 1 mM NaN_3 or 0.06% LDAO, as specified. (B) Samples, 2 μg each of the wild-type or reduced mutant enzyme, were injected into 1 mL of assay medium containing 2 mM ATP plus 3 mM Mg^{2+} with or without 0.06% LDAO, as indicated. Recording was initiated within 3 s after injecting enzyme. The numbers on the traces represent the final rates of ATP hydrolysis recorded over the last 1 min of each assay expressed in micromoles of ATP hydrolyzed per milligram per minute.

Figure 1A also illustrates turnover-dependent inhibition that occurs when the subcomplexes hydrolyze 50 μM ATP in the presence of 1 mM NaN_3. Azide is thought to stabilize inhibitory MgADP bound to a catalytic site, thus preventing release when ATP binds to noncatalytic sites (*23*). In contrast, Figure 1A shows that a single, rapid rate is observed when the wild-type and fully reduced mutant enzymes hydrolyze 50 μM ATP in the presence of 0.06% LDAO. The nonionic detergent prevents turnover-dependent entrapment of inhibitory MgADP in a catalytic site (*23*). It is interesting that the fully reduced mutant enzyme is stimulated nearly 6-fold by LDAO, whereas the wild-type enzyme is stimulated 4-fold under the same conditions. This suggests that the reduced mutant enzyme has higher propensity than wild type to entrap inhibitory MgADP in a catalytic site during turnover.

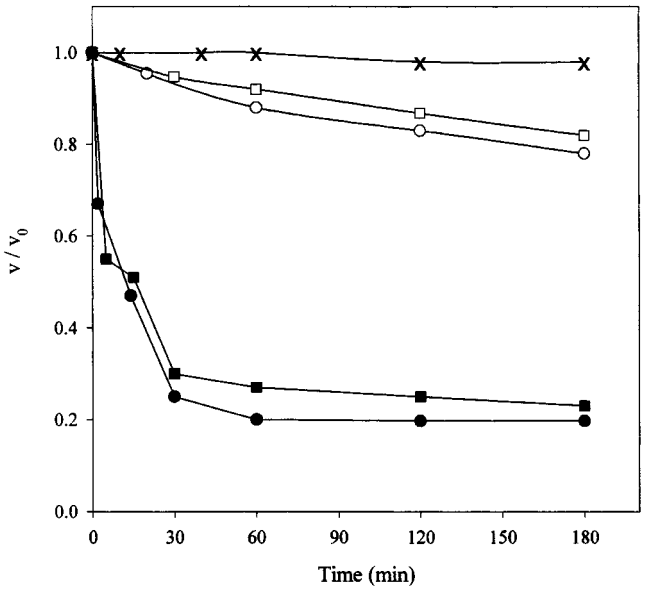

FIGURE 2: Time-dependent inactivation of the reduced $(\alpha F^{357}C)_3(\beta R^{372}C)_3\gamma$ mutant enzyme by $CuCl_2$ under various conditions. The fully reduced double mutant was prepared as described under Experimental Procedures. Immediately before addition of $CuCl_2$, DTT was removed from the reduced enzyme by passing it through Sephadex G-50 centrifuge columns equilibrated with 50 mM Tris-HCl, pH 8.0. Samples of the enzyme prepared in this manner were incubated at 1 mg/mL with the following additions before assaying 3 μL samples at the times indicated: (×) 10 mM DTT; (open circles) none; (closed circles) 10 μM Cu^{2+}; (open squares) 3.1 μM ADP and 1 mM $MgCl_2$; (closed squares) 3.1 μM ADP and 1 mM $MgCl_2$ followed by 10 μM $CuCl_2$.

Figure 1B compares hydrolysis of 2 mM ATP by the wild-type and mutant enzymes in the presence and absence of LDAO. Both traces are curved upward, indicating that entrapment of inhibitory MgADP also occurs under these conditions. The trace for the reduced double mutant shows more pronounced deceleration, which also indicates that it is more susceptible to inhibition by inhibitory MgADP.

The $(\alpha F^{357}C)_3(\beta R^{372}C)_3\gamma$ Subcomplex Retains Attenuated ATPase Activity with Altered Characteristics after Cross-Linking α and β Subunits at Two Noncatalytic Site Interfaces. Figure 2 shows that treatment of the fully reduced mutant subcomplex with 10 μM $CuCl_2$ at 23 °C in the absence of DTT (closed circles) led to a slow decrease of ATPase activity that plateaus at 80% inactivation after about 45 min. Further inactivation was not observed for at least 16 h. Addition of 100 μM $CuCl_2$ to the reduced enzyme led to nearly instantaneous loss of ATPase activity to the same level where it remained unchanged after 16 h (data not shown). Binding MgADP to a single catalytic site had no effect on the rate or extent of inactivation of the enzyme with 10 μM $CuCl_2$ (closed squares). However, in experiments not illustrated, it was observed that 200 μM MgADP significantly slowed inactivation and 5 mM MgADP nearly completely prevented inactivation induced by 10 μM $CuCl_2$.

In the absence of DTT, the reduced enzyme was inactivated slowly in the presence (open squares) or absence (open circles) of MgADP bound to a single catalytic site. No activity was lost when the reduced enzyme was incubated with EDTA in the absence of DTT, suggesting that the observed inactivation represents autoxidation catalyzed by metal ion contaminants in the buffer (data not shown).

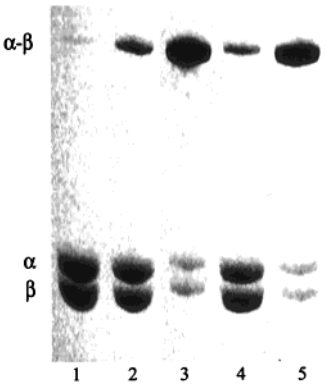

FIGURE 3: Comparison of the formation of α−β cross-links revealed on SDS−PAGE before and after oxidation of the reduced mutant in the presence or absence of MgADP. After incubating the reaction mixtures described in Figure 1 for 3 h at 23 °C, 5 μg samples of each were submitted to SDS−PAGE on 12% gels at 200 V cm^{-1}. The gel was stained with Coomassie Brilliant Blue R250. The samples contained the fully reduced enzyme plus (lane 1) 10 mM DTT, (lane 2) no additions, (lane 3) 10 μM $CuCl_2$, (lane 4) 3.1 μM ADP and 1 mM $MgCl_2$, and (lane 5) 3.1 μM ADP and 1 mM $MgCl_2$ followed by 10 μM $CuCl_2$.

Figure 3 shows the extent of cross-linking between α and β subunits observed after samples of the reaction mixtures described in Figure 2 were submitted to SDS−PAGE. It is clear that free α and β subunits remained after the enzyme samples in lanes 3 and 5 were inactivated by 80% in the presence of 10 μM $CuCl_2$ for 3 h. Essentially, the same amounts of free α and β subunits were observed when a sample of the double mutant which had been treated with 100 μM $CuCl_2$ for 16 h at 23 °C was submitted to SDS−PAGE (data not shown). After removal of $CuCl_2$ from enzyme oxidized under these conditions, titration of the residual unmodified cysteine with DTNB showed that 0.4 mol of free sulfhydryl groups remained per mole of enzyme (*21*). From these results it is concluded that after disulfide bonds are formed between at least two noncatalytic site interfaces, the mutant enzyme hydrolyzes 2 mM ATP at about 20% of the rate exhibited by the fully reduced mutant enzyme. This is 10% of the rate exhibited by the wild-type enzyme.

Panels A and B of Figure 4 illustrate hydrolysis of 50 μM and 2 mM ATP, respectively, by the $(\alpha F^{357}C)_3(\beta R^{372}C)_3\gamma$ subcomplex after it was inactivated by 80% with $CuCl_2$. The trace obtained upon hydrolysis of 50 μM ATP by the cross-linked double mutant in the absence of additions illustrated in Figure 4A differs considerably from the trace recorded in Figure 1A for the reduced enzyme under the same conditions. The trace obtained with the cross-linked enzyme is biphasic rather than triphasic. No acceleration from the inhibited rate was observed when the trace was extended an additional 6 min over that illustrated in Figure 4A. Therefore, after the initial burst, ATPase activity occurs at 10% of the initial rate and does not accelerate to a third kinetic phase. This suggests that, after cross-linking, either the mutant enzyme does not bind nucleotides to noncatalytic sites or that it binds nucleotides to noncatalytic sites without promoting dissociation of inhibitory MgADP from the affected catalytic site.

In the presence of 1 mM NaN_3, the cross-linked enzyme hydrolyzes 50 μM ATP with an initial burst that decelerates to a final rate that is 1% of the initial rate, whereas in the

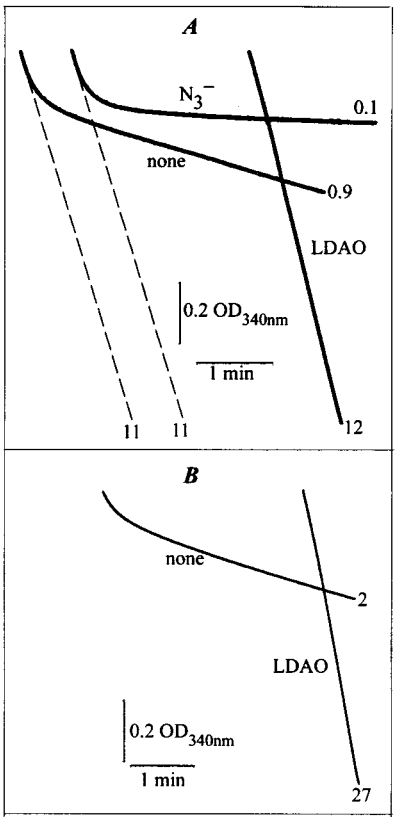

FIGURE 4: Effects of azide and LDAO on hydrolysis of ATP catalyzed by the cross-linked form of the $(\alpha F^{357}C)_3(\beta R^{372}C)_3\gamma$ mutant subcomplex. Continuous assays were performed as described in the legend of Figure 1 except that 10 μg of the cross-linked enzyme was used to initiate hydrolysis of 50 μM ATP (A) and 5 μg of the cross-linked enzyme was used to initiate hydrolysis of 2 mM ATP (B).

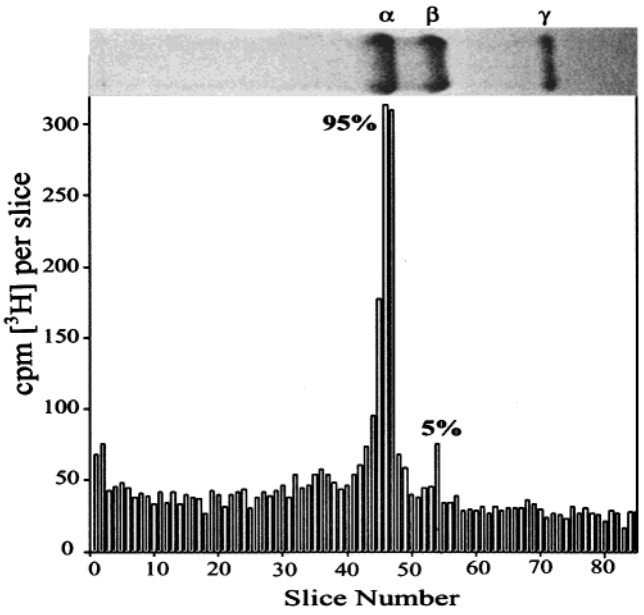

FIGURE 5: Identification of labeled subunits using TDAB−PAGE after activation of the reduced $(\alpha F^{357}C)_3(\beta R^{372}C)_3\gamma$ subcomplex with the iodo[^{3}H]acetate. The [^{3}H]carboxymethylated subcomplex (20 μg), prepared as described under Experimental Procedures and dissolved in 40 μL of 0.2 M NaH_2PO_4 (pH 4.0) containing 6% TDAB and 100 mM β-mercaptoethanol, was submitted to polyacrylamide gel electrophoresis as described in Penin et al. (*22*). Following staining with Brilliant Blue R250, the gel was cut into 1 mm slices that were digested with 15% H_2O_2 for 16 h at 37 °C. The ^{3}H in the digested gel slices was determined by liquid scintillation counting.

presence of 0.06% LDAO, it hydrolyzes 50 μM ATP 13-fold faster than the final rate exhibited in the absence of additions. The dashed lines extending from the initial bursts of the traces obtained with no additions or in the presence of azide show that initial rates observed under these conditions are nearly identical to the linear rate obtained in the presence of LDAO. This supports the contention that LDAO prevents turnover-dependent entrapment of inhibitory MgADP in a catalytic site.

ATPase Activity Is Stimulated after Exclusive Carboxymethylation of the Introduced Cysteines in α *Subunits of the* $(\alpha F^{357}C)_3(\beta R^{372}C)_3\gamma$. Treatment of the fully reduced mutant enzyme with 4 mM iodo[^{3}H]acetate as described under Experimental Procedures led to slow activation of ATPase activity. After 16 h at 23 °C, the specific activity increased from 10 to 20 μmol of ATP hydrolyzed mg^{-1} min^{-1}. When the radioactive, carboxymethylated mutant enzyme was submitted to polyacrylamide gel electrophoresis in the presence of the cationic detergent tetradecyltrimethylammonium bromide (TDAB), it was found that the introduced cysteines in the α subunits were exclusively carboxymethylated (Figure 5). When treated with iodo[^{3}H]acetate under the same conditions, less than 0.2 mol of ^{3}H was incorporated per mole of the wild-type enzyme which contains αC^{193} (corresponds to αC^{201} in MF_1).

After carboxymethylation, the $(\alpha F^{357}C)_3(\beta R^{372}C)_3\gamma$ subcomplex dissociates inhibitory MgADP entrapped in a catalytic site during turnover more readily than the unmodified enzyme. The carboxymethylated enzyme hydrolyzes 50 μM ATP in three distinct kinetic phases (Figure 6A). In contrast, acceleration from the slow, intermediate phase is barely discernible during hydrolysis of 50 μM ATP by the unmodified mutant enzyme (Figure 1A). Moreover, in the presence of LDAO, the rate of hydrolysis of 2 mM ATP by the carboxymethylated enzyme is stimulated only 3-fold (Figure 6B), rather than 6-fold as observed for the unmodified mutant enzyme (Figure 1B). However, hydrolysis of 50 μM ATP by the carboxymethylated mutant enzyme is stimulated 6-fold rather than 3-fold. This may reflect that carboxymethylation lowers the affinity of catalytic sites for MgATP. The K_m values estimated from Lineweaver−Burk plots (data not shown) for the unmodified and carboxymethylated mutant enzymes were 34 and 109 μM, respectively.

Noncatalytic Sites in the Unmodified and Modified $(\alpha F^{357}C)_3(\beta R^{372}C)_3\gamma$ *Subcomplex Are Photolabeled with 2-*N_3*-[*^{3}*H]ADP*. To determine whether carboxymethylation or formation of cross-links between the introduced cysteines in the $(\alpha F^{357}C)_3(\beta R^{372}C)_3\gamma$ subcomplex affects affinity of noncatalytic sites for nucleotides, the reduced, carboxymethylated, and cross-linked forms of the enzyme were photolabeled with 2-N_3-[^{3}H]ADP. Figure 7 compares profiles of radioactive peptides resolved when tryptic digests of the three photolabeled forms of the enzyme were submitted to HPLC. In each case, two major peaks of radioactivity eluted from the column. By analogy with HPLC profiles obtained after photolabeling the wild-type subcomplex under analogous conditions (*10*, *24*), the radioactive peak eluting at 80 min represents the tryptic peptide with the sequence β-ALAPEIVGEEH**Y**^{364}QVA **C**^{368}K, where β**Y**^{364} (TF_1 resi-

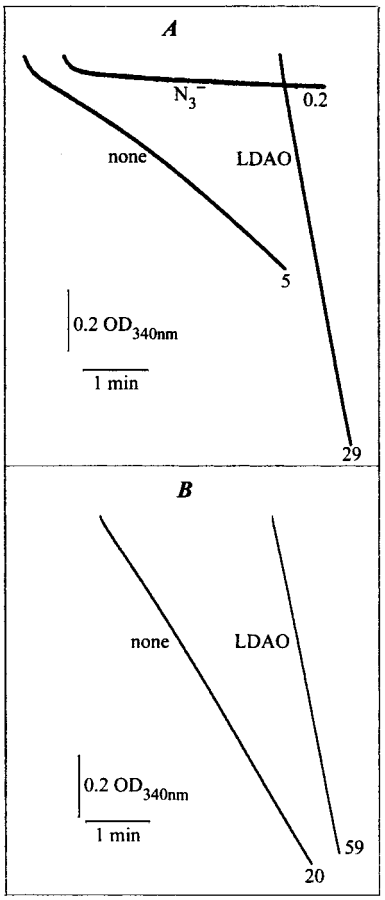

FIGURE 6: Effects of azide and LDAO on hydrolysis of ATP catalyzed by the carboxymethylated form of the $(\alpha F^{357}C)_3(\beta R^{372}C)_3\gamma$ mutant subcomplex. Continuous assays were performed as described in the legend of Figure 1 using 5 μg of the carboxymethylated enzyme to initiate hydrolysis of 50 μM ATP (A) and 2 μg of the carboxymethylated enzyme to initiate hydrolysis of 2 mM ATP (B).

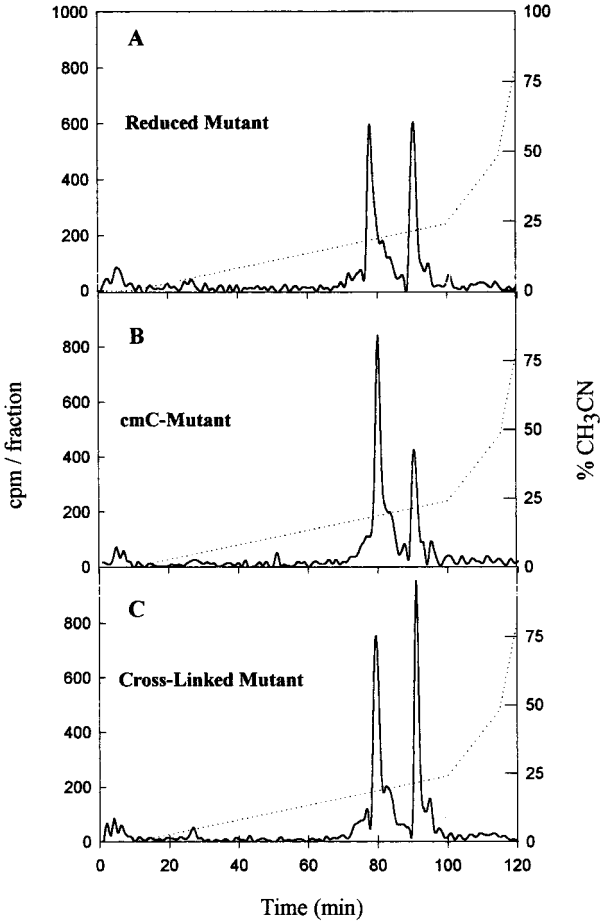

FIGURE 7: Elution profiles of radioactive peptides observed on submitting tryptic digests of the reduced, carboxymethylated, and cross-linked forms of the $(\alpha F^{357}C)_3(\beta R^{372}C)_3\gamma$ mutant subcomplexes to reversed-phase HPLC after photolabeling with 2-N_3-[^{3}H]ADP. Solutions, 1 mL each, containing 1 mg/mL reduced (A), carboxymethylated (cmC mutant) (B), or cross-linked mutant (C) subcomplexes, were incubated with 150 μM 2-N_3-[^{3}H]ADP plus 1 mM $MgCl_2$ at 23 °C in the dark for 20 min, at which time the samples were irradiated and then digested with trypsin as described under Experimental Procedures. Radioactive peptides in the tryptic digests were resolved by HPLC using a C-4 reversed-phase column that was equilibrated with 0.1% HCl and eluted with the gradient of acetonitrile as illustrated. The collected 1 mL fractions were submitted to liquid scintillation counting.

due number) is the residue derivatized with nitreno[^{3}H]ADP and β**C**^{368} (TF_1 residue number) is the introduced cysteine residue in the β subunit derivatized with iodoacetate before the tryptic digest is prepared. The radioactive peak eluting at 92 min represents the tryptic peptide with the sequence β-LAEMGI**Y**^{341}PAVDPLVSTSR, where β**Y**^{341} (TF_1 residue number) is the residue derivatized with nitreno[^{3}H]ADP. From the yield of radioactivity that was recovered in the peak eluted at 80 min, it was estimated that 1.4, 1.7, and 2.0 noncatalytic sites were derivatized with 2-nitreno[^{3}H]ADP in the reduced, carboxymethylated, and cross-linked forms of the $(\alpha F^{357}C)_3(\beta R^{372}C)_3\gamma$ subcomplex, respectively. From the yield of radioactivity in the peak eluting at 92 min it was estimated that 1.0, 0.7, and 1.6 catalytic sites of the reduced, carboxymethylated, and cross-linked forms of the mutant enzyme, respectively, were derivatized with 2-nitreno-[^{3}H]ADP.

DISCUSSION

Given the different arrangements of αF^{357} and βR^{372} at the three α/β interfaces in crystal structures of bovine MF_1 illustrated in Figure 8, it was surprising to find that the $(\alpha F^{357}C)_3(\beta R^{372}C)_3\gamma$ subcomplex retained substantial ATPase activity after disulfide bonds are formed between the introduced cysteines in at least two $\alpha\beta$ pairs. In the original crystal structure of bovine MF_1 (*3*), the side chain of αF^{357} is 4.1 and 4.6 Å from the side chain of βR^{372} at the α_E/β_D and α_D/β_T interfaces, respectively, whereas these side chains are 8.6 Å apart at the α_T/β_E interface as illustrated in Figure 8. These residues are arranged differently in the crystal structure of bovine MF_1 containing two closed catalytic sites with bound $MgADP{\cdot}AlF_4^-$ complexes and the third catalytic site containing bound MgADP in a half-closed conformation (*13*). In this structure, the side chains of αF^{357} and βR^{372} are 4.1 Å apart at the α_E/β_D interface, whereas they are 7.1 and 11 Å apart at the α_D/β_T and α_T/β_E interfaces, respectively. In the absence of LDAO, the steady-state ATPase activity of the cross-linked mutant enzyme is 20% that of the reduced mutant enzyme, whereas in the presence of LDAO, the ATPase activity of the cross-linked enzyme is 47% that of the reduced enzyme. Therefore, the extreme heterogeneity of the relative positions of the side chains of αF^{357} and βR^{372} observed in crystal structures of bovine MF_1 may reflect adjustments of the overall conformations of enzyme mol-

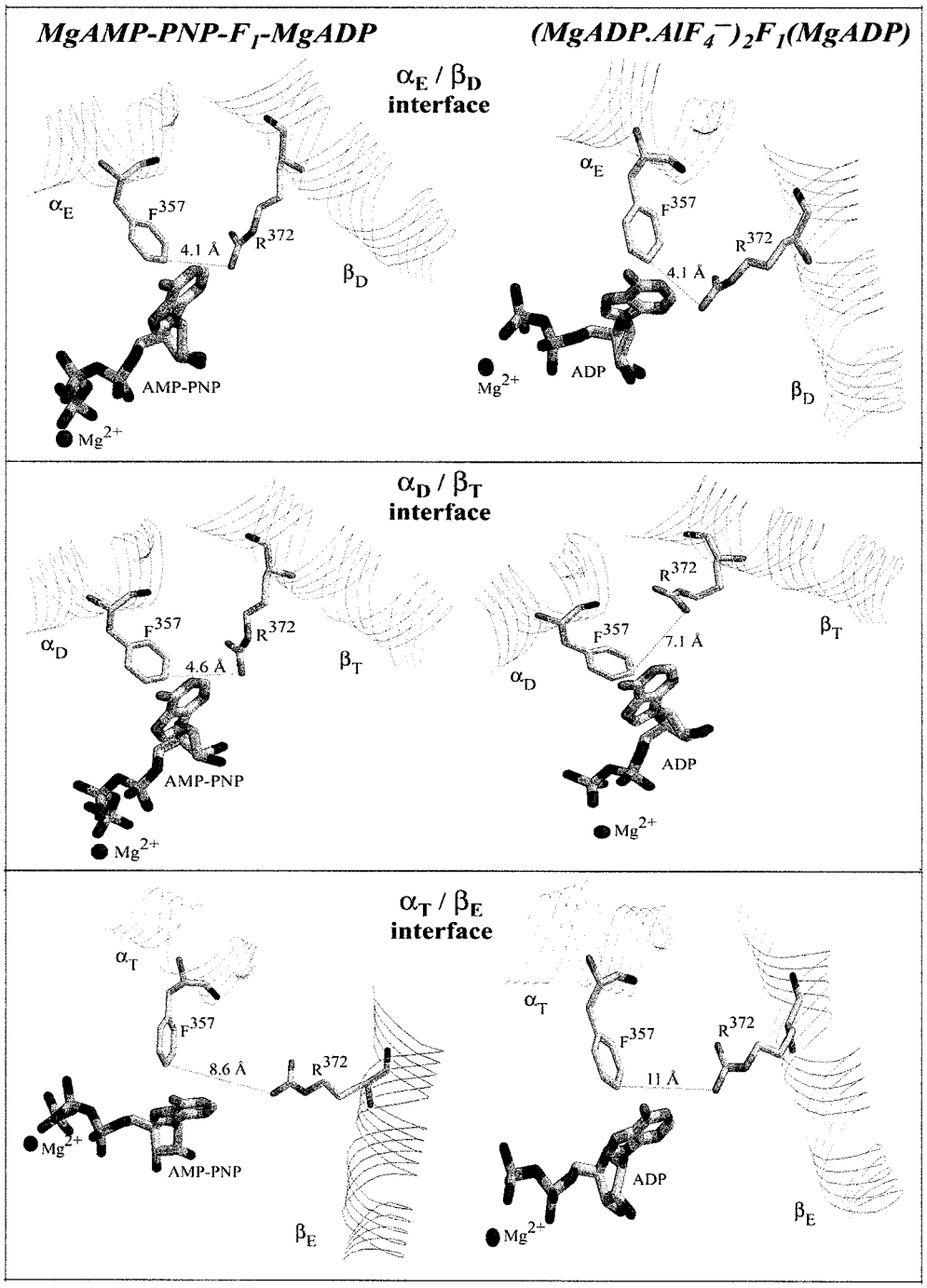

FIGURE 8: Different arrangements of the side chains of αF^{357} and βR^{372} at noncatalytic site interfaces in crystal structures of bovine heart MF_1. On the left are the nearest distances between the side chains of αF^{357} and βR^{372} at the α_E/β_D, α_D/β_T, and α_T/β_E interfaces in the original crystal structure of MF_1 from bovine heart designated MgAMP-PNP−F_1−MgADP (*3*). On the right are the nearest distances between the side chains of αF^{357} and βR^{372} at the α_E/β_D, α_D/β_T, and α_T/β_E interfaces in the crystal structure of MF_1 in which two catalytic sites in closed conformations contain MgADP−fluoroaluminate complexes and the third catalytic site in a half-closed conformation contains MgADP (*13*). This structure is designated $(MgADP{\cdot}AlF_4^-)_2F_1(MgADP)$.

ecules when they are packed in crystal lattices rather than conformational states through which they must pass during catalysis.

Unlike the wild-type enzyme and unmodified and carboxymethylated forms of the mutant enzyme, the cross-linked mutant enzyme entraps inhibitory MgADP during turnover when assayed in the absence of LDAO that is not released under conditions wherein binding of ATP to noncatalytic sites of the wild-type enzyme promotes release of MgADP from the affected catalytic site. Since the noncatalytic sites of the $(\alpha F^{357}C)_3(\beta R^{372}C)_3\gamma$ subcomplex are photolabeled to about the same extent with 2-N_3-ADP before and after cross-linking, decreased affinity of noncatalytic sites for MgATP does not appear to be responsible for the diminished release of inhibitory MgADP observed when the cross-linked enzyme hydrolyzes 2 mM ATP.

To explain transient entrapment of inhibitory MgADP in a single catalytic site during ATP hydrolysis catalyzed by MF_1, it has been postulated that an active or readily activatable $F_1{\cdot}$(MgADP) complex is in equilibrium with an inactive $F_1{*}{\cdot}$(MgADP) complex (*25*, *26*). Inhibition by azide, which is also turnover-dependent, is thought to perturb the

equilibrium by stabilizing the F_1*•(MgADP) complex (*23*, *25*, *27*, *28*). However, for another opinion on the mechanism of inhibition of F_1-ATPases by azide see Weber and Senior (*29*). Mutant $\alpha_3\beta_3\gamma$ subcomplexes of TF_1, including the unmodified and cross-linked forms of the $(\alpha F^{357}C)_3$-$(\beta R^{372}C)_3\gamma$ subcomplex described here, that have higher propensity than wild type to entrap inhibitory MgADP in a catalytic site during turnover are stimulated to a greater extent than wild type when assayed in the presence of LDAO (*10*, *30*, *31*). In contrast, those mutant enzymes that have lower propensity than wild type to entrap inhibitory MgADP in a catalytic site during turnover, including the carboxymethylated $(\alpha F^{357}C)_3(\beta R^{372}C)_3\gamma$ subcomplex described here, exhibit lower sensitivity to azide and are stimulated to a lesser extent or slightly inhibited by LDAO (*23*, *31*, *32*).

It has been shown that the ATPase activities of the $\alpha_3\beta_3$ and $\alpha_3\beta_3\delta$ subcomplexes of TF_1 are neither inhibited by azide nor activated by LDAO, suggesting that the γ subunit participates in the F_1•(MgADP) $\leftrightarrows$ F_1*•(MgADP) equilibrium (*33*). The conformation of the γ subunit in the revised crystal structure of EF_1 recently reported by Hausrath et al. (*34*) suggests a possible connection between activation of bacterial F_1-ATPases by LDAO and the conformation of the γ subunit. According to the new interpretation of the electron density map, the coiled coil comprised of the N- and C-terminal α helices found in crystal structures of MF_1 is partially unwound and the ϵ subunit is folded in the ATPase-inhibitory "up" conformation described by Tsunoda et al. (*35*). In the up conformation, the C-terminal α helix of ϵ is perpendicular to its β sandwich domain and interacts with the DELSEED loop in the C-terminal, α-helical domain of one of the β subunits. To explain the F_1•(MgADP) $\leftrightarrows$ F_1*•(MgADP) described above, we postulate that the α helices in the coiled coil of γ are fully wound in the F_1•(MgADP) state, whereas they are partially unwound in the F_1*•(MgADP) state. It is further postulated that interactions between adjacent side chains of the constituent α helices that stabilize the coiled coil of γ in the fully wound conformation find new partners within the $\alpha_3\beta_3$ hexamer upon unwinding that stabilize the conformation observed in the crystal structure of EF_1. To account for the absence of turnover-dependent entrapment of inhibitory MgADP during ATP hydrolysis in the presence of LDAO, it is proposed that the nonionic detergent favors the wound conformation by destabilizing interactions between side chains of γ in the partially unwound form, with side chains extending from the $\alpha_3\beta_3$ hexamer.

To explain why ATP synthesis in submitochondrial particles or artificial membranes containing TF_oF_1 and bacteriorhodopsin is not affected by preloading a catalytic site with MgADP (*35*, *36*), we take into account the generally accepted assumption that during ATP synthesis, the proton electrochemical gradient drives clockwise rotation of the γ subunit (*15*, *38*, *39*). Under these conditions, the torque imposed by the electrochemical gradient should force the N- and C-terminal α helices of the γ subunit into the fully wound conformation. Consistent with this argument, Fischer et al. reported that the *E. coli* ATP synthase reconstituted into liposomes containing bound MgADP and P_i has low ATPase activity in the absence of energization with an artificially imposed proton electrochemical potential. After energization, the initial rate of ATP hydrolysis catalyzed by the proteoliposomes increased 9-fold (*40*).

REFERENCES

1. Boyer, P. D. (1997) *Annu. Rev. Biochem. 66*, 717−749.
2. Nakamoto, R. K., Ketchum, C. J., and Al-Shawi, M. K. (2000) *Annu. Rev. Biophys. Biomol. Struct. 28*, 205−234.
3. Abrahams, J. P., Leslie, A. G. W., Lutter, R., and Walker, J. E. (1994) *Nature 370*, 621−628.
4. Esch, F. S., and Allison, W. S. (1978) *J. Biol. Chem. 253*, 6100−6106.
5. Bullough, D. A., Yoshida, M., and Allison, W. S. (1986) *Arch. Biochem. Biophys. 244*, 865−871.
6. Matsuno-Yagi, A., and Hatefi, Y. (1984) *Biochemistry 23*, 3508−3514.
7. Milgrom, Y. M., Ehler, L. L., and Boyer, P. D. (1990) *J. Biol. Chem. 265*, 18725−16728.
8. Jault, J.-M., and Allison, W. S. (1993) *J. Biol. Chem. 269*, 319−325.
9. Paik, S. R., Jault, J-. M., and Allison, W. S. (1994) *Biochemistry 33*, 126−133.
10. Jault, J.-M., Matsui, T., Jault, F. M., Kaibara, C., Muneyuki, E., Yoshida, M., Ohta, T., Kagawa, Y., and Allison, W. S. (1995) *Biochemistry 34*, 16412−16418.
11. Matsui, T., Muneyuki, E., Honda, M., Allison, W. S., Dou, C., and Yoshida, W. S. (1997) *J. Biol. Chem. 272*, 8215−8221.
12. Gibbons, C., Montgomery, M. G., Leslie, A. G. W., and Walker, J. E. (2000) *Nat. Struct. Biol. 7*, 1055−1061.
13. Menz, R. I., Walker, J. E., and Leslie, A. G. W. (2001) *Cell 106*, 331−341.
14. Noji, H., Yasuda, R., Yoshida, M., and Kinosita, K., Jr. (1997) *Nature 386*, 299−302.
15. Yasuda, R., Noji, H., Kinosota, K., and Yoshida, M. (1998) *Cell 93*, 1117−1124.
16. Allison, W. S., Ren, H., and Dou, C. (2000) *J. Bioenerg. Biomembr. 32*, 531−538.
17. Matsui, T., and Yoshida, M. (1995) *Biochim. Biophys. Acta 1231*, 139−146.
18. Penefsky, H. S. (1977) *J. Biol. Chem. 252*, 2891−2899.
19. Bullough, D. A., Verburg, J. G., Yoshida, M., and Allison, W. S. (1987) *J. Biol. Chem. 262*, 1165−11683.
20. Bradford, M. M. (1976) *Anal. Biochem. 72*, 248−254.
21. Ellman, G. L. (1959) *Arch. Biochem. Biophys. 82*, 70−77.
22. Penin, F., Godinot, C., and Gautheron, D. C. (1984) *Biochim. Biophys. Acta 775*, 239−245.
23. Jault, J.-M., Dou, C., Grodsky, N. B., Matsui, T., Yoshida, M., and Allison, W. S. (1996) *J. Biol. Chem. 271*, 28818−28824.
24. Jault, J.-M., Kaibara, C., Yoshida, M., Garrod, S., and Allison, W. S. (1994) *Arch. Biochem. Biophys. 310*, 282−288.
25. Vasileva, E. A., Minkov, I. B., Fitin, A. F., and Vinogradov, A. D. (1982) *Biochem. J. 202*, 9−14.
26. Milgrom, Y. M., and Murataliev, M. B. (1989) *Biochim. Biophys. Acta 975*, 50−58.
27. Murataliev, M. B. (1992) *Eur. J. Biochem. 31*, 12885−12892.
28. Hyndman, D. J., Milgrom, Y. A., Bramhall, E. A., and Cross, R. L. (1994) *J. Biol. Chem. 269*, 28871−28877.
29. Weber, J., and Senior, A. E. (1998) *J. Biol. Chem. 273*, 33210−33215.
30. Grodsky, N. B., Dou, C., and Allison, W. S. (1998) *Biochemistry 37*, 1007−1014.
31. Ren, H., and Allison, W. S. (2000) *J. Biol. Chem. 275*, 10057−10063.
32. Dou, C., Fortes, P. A. G., and Allison, W. S. (1998) *Biochemistry 37*, 16757−16764.
33. Paik, S. R., Yokoyama, K., Yoshida, M., Ohta, T., Kagawa, Y., and Allison, W. S. (1993) *J. Bioenerg. Biomembr. 25*, 679−684.
34. Hausrath, A. C., Capaldi, R. A., and Matthews, B. W. (2001) *J. Biol. Chem.* (in press).
35. Tsunoda, S. P., Rodgers, A. J. W., Aggeler, R., Wilce, M. C. J., Yoshida, M., and Capaldi, R. A. (2001) *Proc. Natl. Acad. Sci. U.S.A. 98*, 6560−6564.
36. Vinogradov, A. D. (2000) *J. Exp. Biol. 203*, 41−49.

37. Bald, D., Amano, T., Muneyuki, E., Pitard, B., Rigaud, J.-L., Kruip, J., Hisabori, T., Yoshida, M., and Shibata, M. (1998) *J. Biol. Chem. 273*, 865−870.
38. Sambongi, Y., Iko., Y., Tanabe, M., Omote, H., Iwamoto-Kihara, A., Ueda, I., Yanagida, T., Wada, Y., and Futai, M. (1999) *Science 286*, 1772−1774.
39. Hutcheon, M. L., Duncan, T. M., Ngai, H., and Cross, R. L. (2001) *Proc. Natl. Acad. Sci. U.S.A. 98*, 8519−8524.
40. Fischer, S., Gräber, P., and Turina, P. (2000) *J. Biol. Chem. 275*, 30157−30162.

BI0120291